Experimental and numerical study on crashworthiness of cold-formed dimpled steel columns

Ce Liang [a,*] Chang Jiang Wang [a], Van Bac Nguyen [b], Martin English [c], Diane Mynors [a]

[a] Department of Engineering and Design, University of Sussex, Sussex House, Brighton, BN1 9RH, United Kingdom

[b] College of Engineering and Technology, University of Derby, Markeaton Street, Derby, DE22 3AW, United Kingdom

[c] Hadley Group Technology, Hadley Industries plc, Downing Street, Smethwick, West Midlands B66 2PA, United Kingdom

[*] Corresponding author at: Richmond Building, Department of Engineering and Design, University of Sussex, Brighton BN1 9QT, United Kingdom. *Email address: cl305@sussex.ac.uk*

Abstract

The UltraSTEEL® forming process forms plain steel sheets into dimpled steel sheets and this process increases the sheet material's strengths by generating plastic deformation on the material during the process. This paper presented experimental testing and developed a finite element (FE) model to predict the energy absorption characteristics of dimpled thin-walled structures under axial impact loads, and compared the energy absorption efficiencies (specific energy absorption) of plain and dimpled columns. Dynamic experimental tests were conducted using the drop tower at two different impact velocities. Explicit FE analysis were then carried out to simulate the experiments. The FE method was validated by comparing the numerical and experimental failure modes, crushing force response and specific energy absorptions. The validated FE method was then applied in an optimization study on the parameter of forming depth. The effects of forming depth on both geometry and material properties have been taken into account in the optimization study. It has been found that the specific energy absorption of dimpled columns is up to 16.3% higher than the comparable plain columns.

Keywords

Explicit dynamics finite element analysis; UltraSTEEL; Axial crushing; Energy absorption

1. Introduction

Thin-walled structures are widely used as kinetic energy absorbers in sea, land and air vehicles for their light weight, high energy absorbing capacity and low cost [1]. Among various types of loads, axial crushing is one of the most typical loading conditions that thin-walled columns are designed to carry. When subjected to an axial crushing load, thin-walled columns can absorb a large amount of energy through plastic deformation [1]. Wierzbicki and Abramowicz [1] proposed the super folding element (SFE) theory to predict the crush response of thin-walled columns. Many researchers have also studied the crushing mechanisms of thin-walled columns being crushed [1-4].

In recent years, there is a particular interest in improving the crashworthiness of thin-walled structures from different angles. Some studies focused on thin-walled columns with innovative cross-sections [5-15]. By contrast, some studies focused on columns made of high strength materials [16-19], or filled by different materials [20-22]. Tang et al. [5] proposed a new strategy to increase the energy absorption capacity of thin-walled columns by introducing non-convex corners in cross sections. Abbasi et al. [6, 7] extended this strategy by carrying out numerical and experimental studies on hexagonal, octagonal and 12-edge section columns' response to both quasi-static and dynamic axial crushing loads. The numerical results were validated by comparing to experimental results in terms of failure mode as well as specific energy absorption (SEA). It was claimed that the SEA of 12-edge section column was the highest among the three sections. According to Abbasi et al. [7], a good agreement between numerical and experimental results in terms of SEA was achieved, where difference was smaller than 8.6%. Jusuf et al. [8] numerically and experimentally studied the response of prismatic multi-cell section columns to dynamic crushing loads. It was

suggested that comparing to double wall structure with the same mass, the mid-rib cross-section structure had a 91.2% higher mean crushing force. Qiu et al. [9] used FE method to predict the response of hexagonal multi-cell columns to off-axis quasi-static loads. Tran et al. [10] proposed the triangular multi-cell and employed the SFE method to optimize the geometric parameters. A similar approach was adopted to optimize the geometric parameters of angle element multi-cell structures [11]. Zhang and Zhang [12] conducted a similar study to optimize the geometric parameters of quadruple cell section columns. To validate the FE models, Zhang and Zhang compared the numerical results with both experimental and theoretical results [12]. It was claimed that the simulation errors were smaller than 4.40% and 8.40% in terms of mean crushing force and peak force, respectively [12]. White et al. [13] theoretically analysed the effect of top-hat and double-hat section columns' geometric parameters on the crush response. Ly et al. [14] then extended the research by using the finite element method and optimized the geometrical parameters of top-hat structures. Zhang et al. [15] modified the conventional closed square section by introducing graded thickness. It was claimed that the introduction of graded thickness can lead to up to 30-35% increase in SEA without increasing the peak force. The simulation errors in their study [15] were up to 12.97% in terms of SEA. Huh and Kang [16] compared the mild steel and high-strength steel columns under quasi-static and dynamic loading conditions, a similar research was done by Schneider and Jones [17]. It was pointed out that for closed square section columns, using high-strength material significantly increased the SEA. Tarigopula et al. [18] focused on the strain rate sensitivity of dual-phase high-strength steel columns, the Cowper-Symonds material model was adopted to characterise materials' strain rate sensitivity. Lam et al. [19] did a case study to analyse the gauge sensitivity of high-strength steel. Hanssen et al. [20] has suggested

empirical equations to theoretically predict the energy absorption performance of foam-filled thin-walled tubes. These empirical equations were then validated by experiments and modified to suit dynamic loading conditions [21]. Zarei et al. [22] pointed out that the foam-filled tube absorbs the same energy while weight was 19% lighter compared with the optimum empty columns through numerical and experimental studies. In the previous studies, two types of triggering mechanisms have been used to initiate the crushing process in simulations. The first type is to create an initial in-extensional geometrical imperfection [8]. The second type is to introduce indentation triggers on the outside plates of the columns [12, 15]. Positions of both types of triggers were the same as those observed in experimental tests [8, 12, 15].

Dimpled steel sheets are cold-roll formed from plain steel sheets by the UltraSTEEL® process developed by Hadley Industries plc [23]. The process uses a pair of rollers with rows of specially shaped teeth that form the dimple shapes from both sides of the plain sheet, as shown in Figure 1 [24]. The dimpled sheet can then be progressively formed into a desired profile by passing through a series of rolls, arranged in tandem, or by press braking. It has been reported through experimental tests and numerical simulations that the strength of dimpled samples was significantly greater than plain samples originating from the same coil material [24-29]. The greater strength of dimpled samples is caused mainly by the work hardening of the material during the dimpling process. In previous articles, the response of open-section dimpled steel columns under quasi-static compression loads has been studied experimentally as well as numerically [27-29]. However, the study only focused on the response of the open section till the buckling point, and the strain rate effect is not taken into account. Finite element simulations of the dimpled columns subjected to dynamic crushing

loads requires validation. The challenge is that the effects of dimpled geometry and non-uniform stress and strain distribution in the dimpled material need to be appropriately represented in the FE models. Additionally, the response of dimpled steel columns to dynamic impact loads has not been investigated yet.

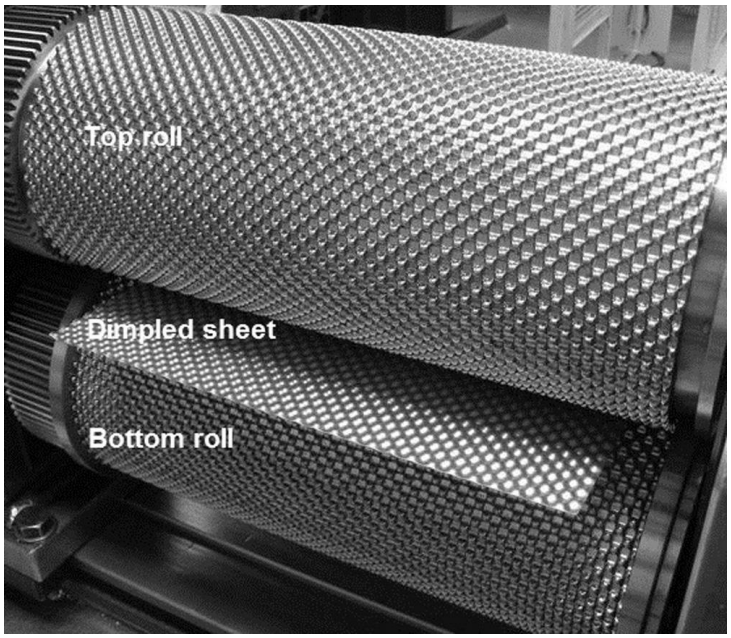

Fig. 1. The UltraSTEEL process and dimpled steel sheet [24]

This paper aims to investigate the finite element modelling method to accurately predict the energy absorption characteristics of dimpled thin-walled columns under dynamic axial crushing loads, as well as analyse the effect of the dimple forming parameters in the UltraSTEEL® process. To achieve this aim, both numerical and experimental studies were carried out on plain and dimpled open-section thin-walled columns under two different impact velocities. Then, finite element simulations were carried out to analyse the effect of the dimpling parameters in the UltraSTEEL® process on the energy absorption characteristics of dimpled thin-walled columns.

2. Method

2.1 Experimental setup

Dynamic crushing tests were carried out at the Warwick Manufacturing Group (WMG) by using INSTRON 9250 drop hammer test machine connected computer control and data acquisition system. Data acquired included instantaneous forces and axial displacements measured at a sampling frequency of 80 kHz, as well as videos taken at 12,500 fps. The schematic plot of the experimental setup is shown in Fig. 2. Two different impact velocities were set as 3.44 m/s and 4.33 m/s, while the impact mass was 168.5 kg. Initiators were introduced when the impact velocity was 4.33 m/s, in order to maintain a consistent failure mode. Tests were repeated for 5 times under each test condition.

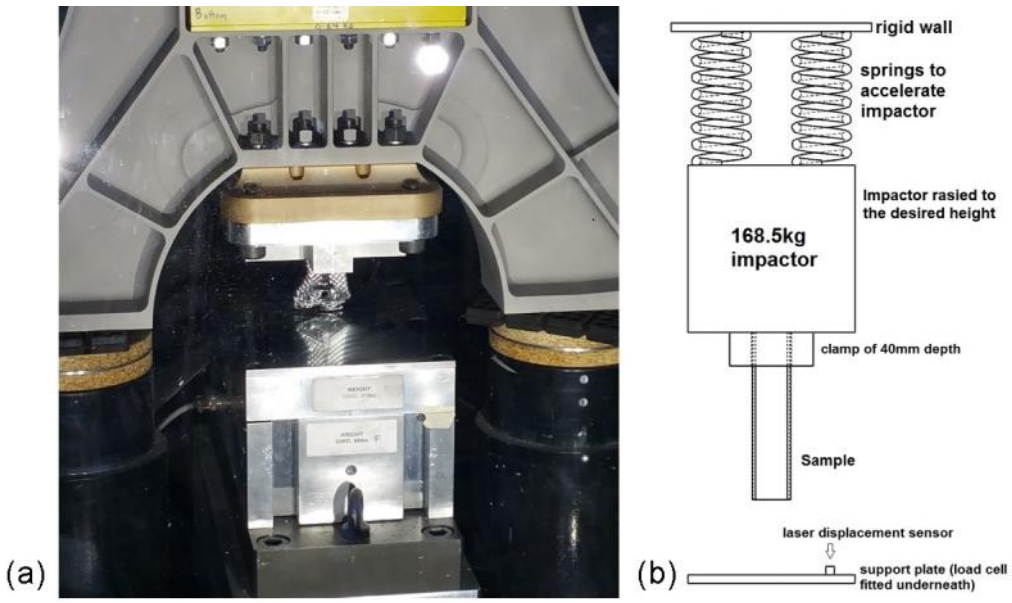

Fig. 2. (a) A photo of the test setup and (b) schematic plot of the test system

The specimens tested in the dynamic crushing tests were made of plain and dimpled galvanised steel. All the specimens originated from the same coil of material. Plain and dimpled specimens are shown in Fig. 3(a). The specimens were fabricated using

band saw-cut techniques. 1mm gauge thickness open section columns were tested. The cross sections of the plain and dimpled specimens are shown in Fig. 3(b), where the gap size d_3 was controlled to be within 1mm and 3mm. The specimens were 200mm long and fixed at one end by clamps with a depth of 40mm, which means the effective axial length was 160mm.

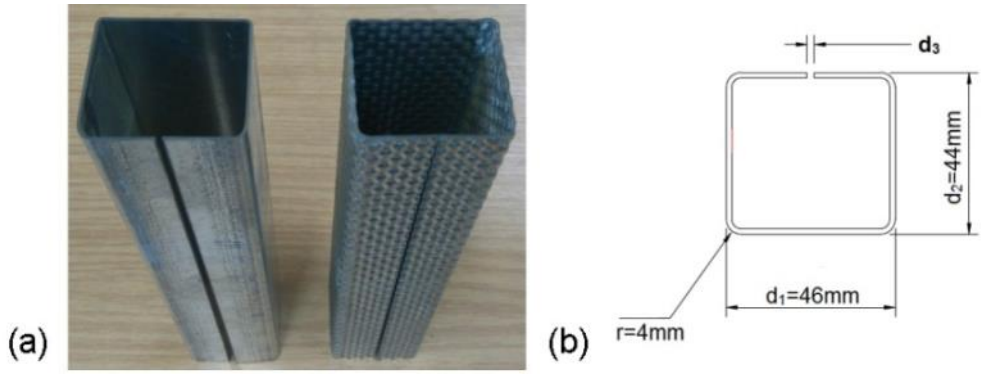

Fig. 3. (a) Plain and dimpled specimens and (b) Cross-sectional dimensions of specimens

The material properties of plain and dimpled steel were determined from quasi-static tensile tests complied with the appropriate British Standard [30]. The quasi-static engineering stress-strain curves of these two materials are shown in Fig. 4. Table 1 shows these two materials' mechanical properties. Details of the tensile test procedure and area measurements are described by Nguyen et al. [26].

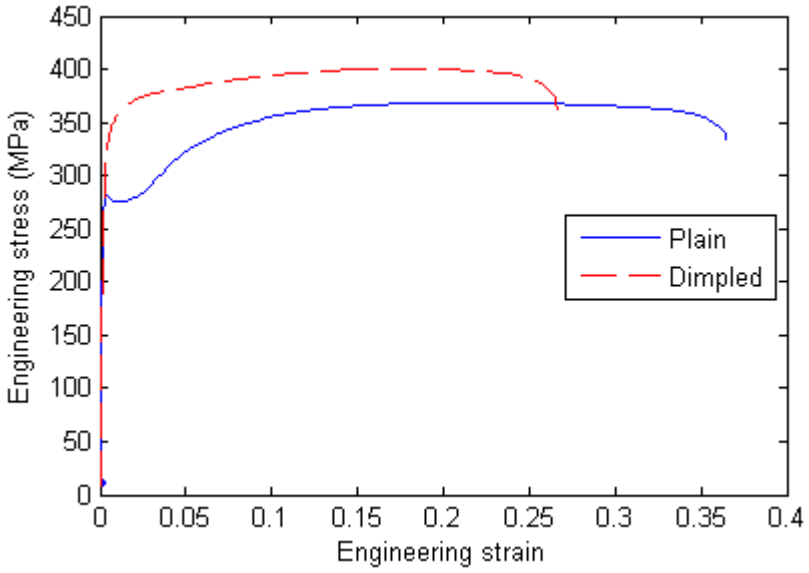

Fig. 4. Quasi-static engineering stress-strain curves of plain and dimpled materials

Table 1. Mechanical properties of plain and dimpled materials

	Young's modulus E (GPa)	**Poisson's ratio**	**Engineering yield strength $\sigma_{y,eng}$(MPa)**	**Engineering Ultimate strength $\sigma_{u,eng}$ (MPa)**
Plain	205	0.3	278	369
Dimpled	205	0.3	325	401

2.2 Numerical modelling

The explicit dynamic finite element analysis code integrated in Ansys Workbench 16.0 [31] was employed to simulate the thin-walled columns' response to dynamic axial impact loads in this study. The solver is suitable for dealing with large deformation and complex contact interaction in crash simulations.

In order to reduce computational time, the dimpled plates were modelled using full-integration shell elements with four nodes and five integration points throughout the thickness. In reality, the thickness of dimpled plate slightly varies at different locations around the dimple valley [24]. However, it was assumed that the thickness was uniform

across the entire plate. The equivalent uniform thickness for dimpled plate was set as 0.9516 mm, which was determined based on the mass conservation of the 1mm gauge plain plate. Additionally, the dimpled material was assumed to be homogeneous in terms of mechanical properties. It can be considered as a two-stage simplification. Stage one was to apply homogeneous material properties instead of non-uniform material properties due to strain hardening during dimple forming. Stage two was to replace solid elements by shell elements, which neglects the stress distribution throughout thickness. It was found that neither of these simplifications has caused a significant change in the simulated stress-strain relationship of the dimpled plates. The UltraSTEEL® process was firstly simulated, using the method introduced by Nguyen et al. [27]. The tensile tests were simulated on FE models with reserved residual stress and strain (solid elements), homogeneous equivalent stress and strain (solid elements) and homogeneous equivalent stress and strain (shell elements). As shown in Fig. 5, the difference between experimental and the numerical model with shell elements and homogeneous material properties can be neglected.

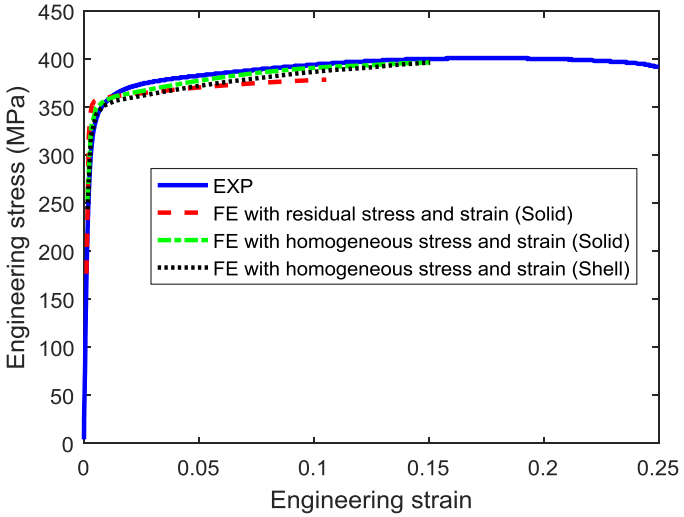

Fig. 5. Experimental and numerical stress-strain curves using different element types and material properties assumptions

True stress and strain were used as shown in equation 1 and 2. The Cowper-Symonds material model was employed to characterise materials' strain rate sensitivity, as shown in equation 3. The true plastic stress-strain curves input to the Ansys programme are shown in Fig. 6.

$$\sigma_{true} = \sigma_{eng}(1 + \varepsilon_{eng}) \tag{1}$$

$$\varepsilon_{true} = \ln(1 + \varepsilon_{eng}) - {}^{\sigma_{eng}}/_{E} \tag{2}$$

$$\sigma^{d} = \left(\sigma_y + B\varepsilon^{n}\right)\left[1 + \left(\frac{\dot{\varepsilon}}{D}\right)^{1/q}\right] \tag{3}$$

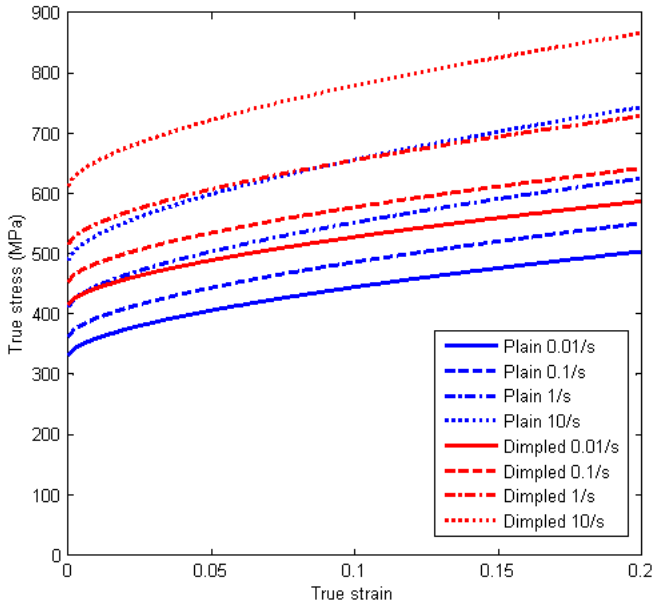

Fig. 6. True stress-strain curves used in simulations with varying strain rates

The selection of element sizes for plain and dimpled models were slightly different. The variation of SEA against the element size for plain models is shown in Fig. 7. The result reveals that SEA have converged when there were 26720 elements on the column, corresponding to a uniform element size of 1 mm. Therefore, the element size was set as 1 mm for plain models. However, smaller elements were necessary for

dimpled models, due to the complicated dimpled geometry. Geometrical distortion can be observed when an element size of greater than 0.55 mm was used (i.e. the maximum allowed element size for dimpled models was 0.55 mm). For dimpled FE models, the difference when using 0.55 mm and 0.275 mm element sizes was negligible in terms of failure mode, peak force and SEA. Therefore, the element size for dimpled models was set as 0.55 mm, which is the smallest element size used in similar studies. This small element size has made the simulations for dimpled models very computational resource consuming, because it not only caused a dramatic increase in the total number of elements, but also reduced the critical time step proportionally in explicit analysis.

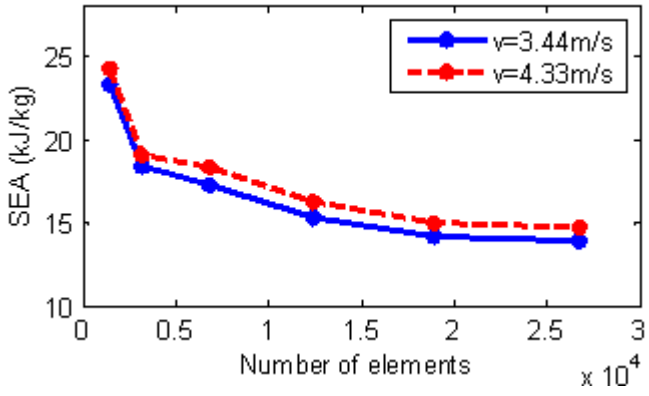

Fig. 7. Element size convergence for plain models

As shown in Fig. 8 and Fig. 9, the FE models for plain and dimpled specimens included the open-section columns and a rigid impactor of 168.5 kg, which was modelled using hexahedral eight-node solid elements. The FE geometrical models were constructed using a single dimple and a bend corner dimple generic models described in [27]. The length for columns were set as 160 mm, which was the effective crushing length in the experiments. All the nodes attached to the bottom of the columns were restrained in

all DOFs. The DOF along x and y axes of the impactor was restrained to ensure that the impactor only moves freely along the longitudinal axis (i.e. z-axis).

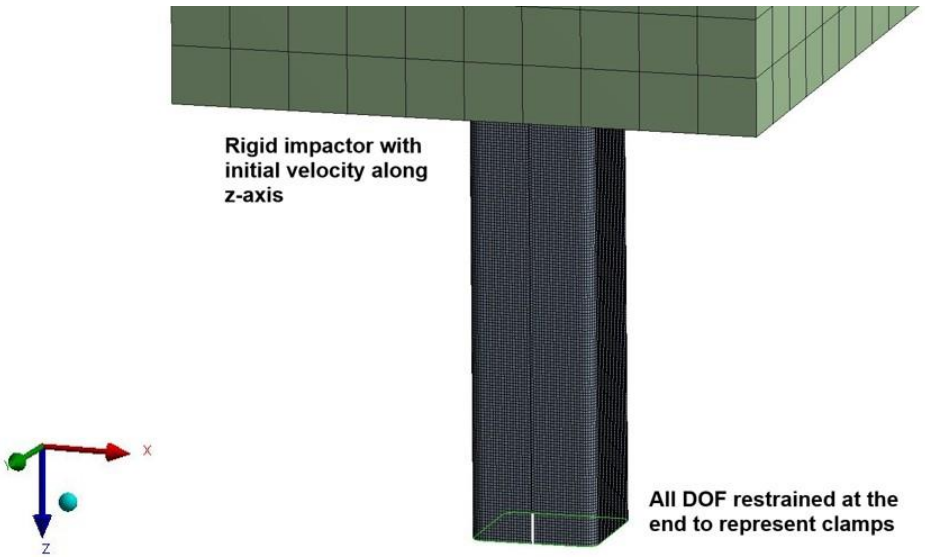

Fig. 8. FE model of plain column

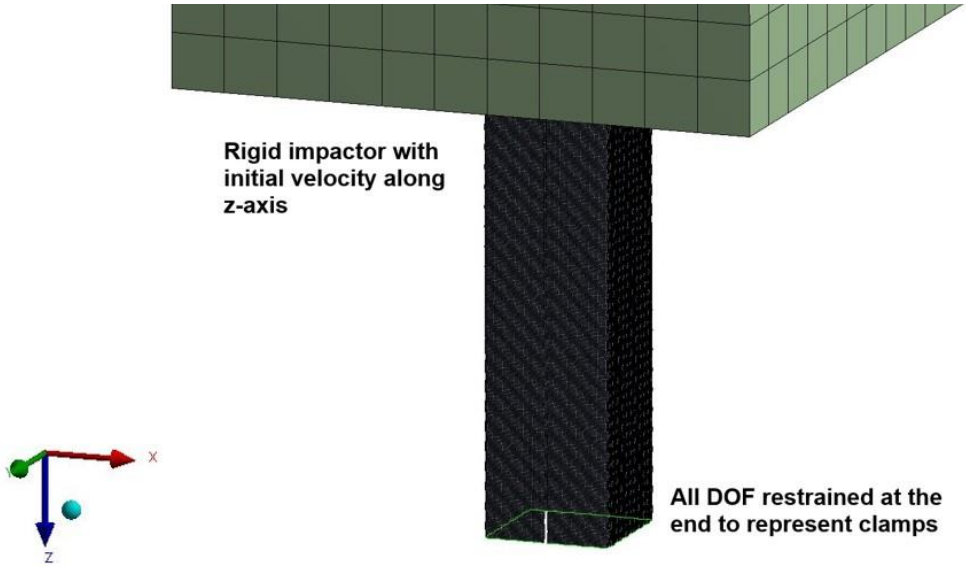

Fig. 9. FE model of dimpled column

In the simulations, triggers were employed to initiate the crushing process. The positions of triggers were set as the position that buckling starts in experimental tests, namely the free end of columns. The effect of introduced triggers is highlighted in Fig. 10 for drop tests with a speed of 3.44 m/s. The numerical initial failure modes with and

without the triggers are shown in Fig. 11. For plain columns, the crushing started from the free end whether the triggers were introduced or not, however the length of the first fold was considerably greater without the triggers. As for dimpled columns, introducing the triggers made the buckling point shifted from a random position to the free end. This difference between plain and dimpled columns indicates that the dimpled columns have higher capacity to prevent flanges from folding inwards or outwards.

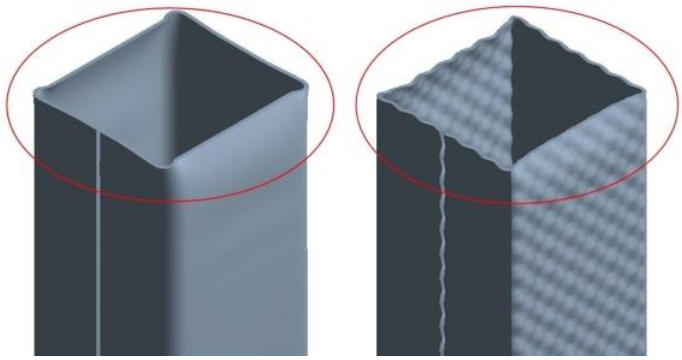

Fig. 10. Plain and dimpled columns after introducing triggers

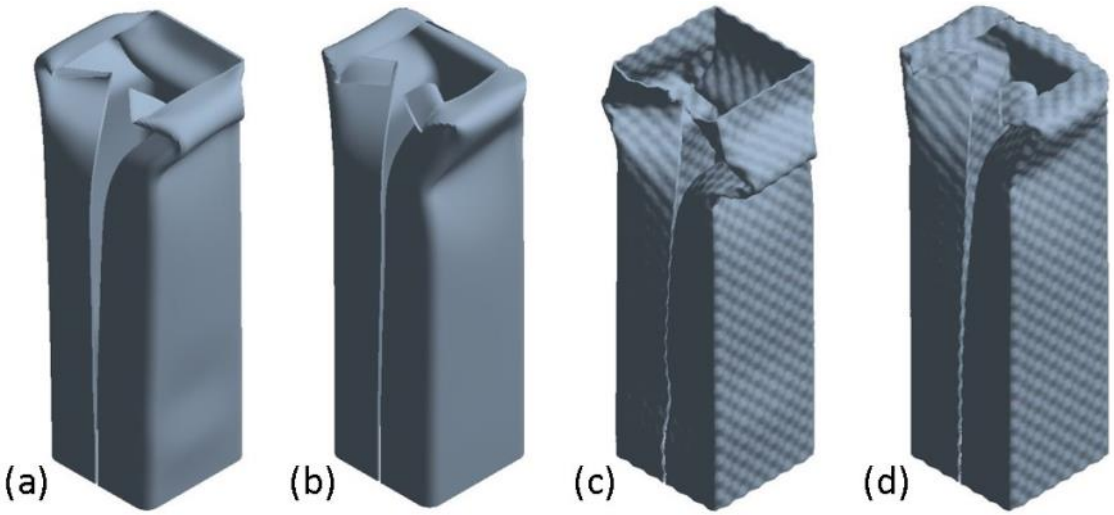

Fig. 11. Initial failure modes of (a) plain column without triggers, (b) plain column with triggers, (c) dimpled column without triggers and (d) dimpled columns with triggers

3. Validation of the FE method

3.1 Experimental results

As mentioned in section 2.1, band saw-cut specimens were used to analyse the energy absorption characteristics for their inherent imperfections. However, due to the uncertainty of this inherent imperfection, asymmetric crushing modes may occur after several layers of folds have been formed (i.e. the crushed columns tend to slide towards one side), as illustrated in Fig. 12. It has been observed that dimpled columns performed better at resisting the “side-sliding”. When the impact velocity was 4.33 m/s, 4 out of 5 plain specimens experienced noticeable side-sliding, while only 1 out of 5 dimpled specimens experienced noticeable side-sliding.

Fig. 12. Asymmetrically crushed specimens due to inherent imperfection

For band saw-cut specimens, the typical crushing modes at the two impact velocities (3.44 m/s and 4.33 m/s) are shown in Fig. 13. The 40mm deep clamps have prevented the flanges from folding outwards. Therefore, the folding mechanism of the tested open section specimens were very similar to closed square section columns. Moreover, the introduced dimpled geometry did not cause significant difference in global failure modes.

Fig. 13. Typical deformed shapes of tested specimens

The experimental force – axial displacement curves and energy absorbed (EA) – axial displacement curves are shown in blue in Fig. 14. In this study, specific energy absorption (SEA) was employed as the primary index to evaluate the energy absorption performance. SEA is calculated based on the effective crushing distance and it is defined as equation 4, where δ represents the axial displacement, P represents the instantaneous crushing force, and m represents the mass of the deformed column.

$$SEA = \frac{\int_0^{\delta_{total}} P d\delta}{m} = \frac{EA\ per\ unit\ length\ of\ axial\ displacement}{Mass\ of\ column\ per\ unit\ length} \quad (4)$$

In equation 3, the term '$EA\ per\ unit\ length\ of\ axial\ displacement$' equals to the gradient of Energy absorbed – axial displacement curves, while the term '$Mass\ of\ column\ per\ unit\ length$' is a constant which can be easily measured. Therefore, linear fitting was carried out in order to determine the term '$EA\ per\ unit\ length\ of\ axial\ displacement$'. Median values of test results were taken in order to eliminate those off-the-mark results. Table 2 shows the experimental results. Mean crushing forces P_m are proportional to specific energy absorptions SEA because the mass of all specimens were the same.

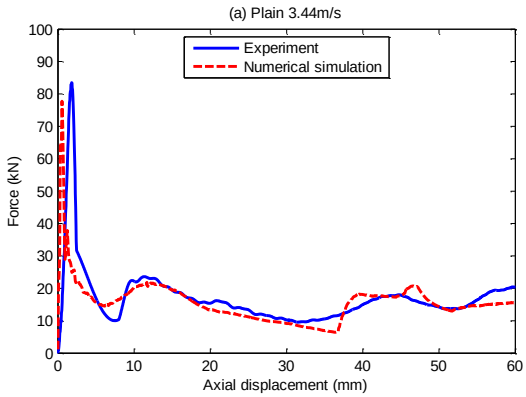
(a) Plain 3.44m/s
Experiment
Numerical simulation
Force (kN)
Axial displacement (mm)

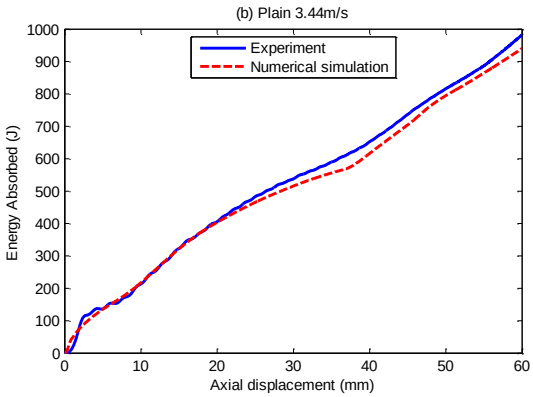
(b) Plain 3.44m/s
Experiment
Numerical simulation
Energy Absorbed (J)
Axial displacement (mm)

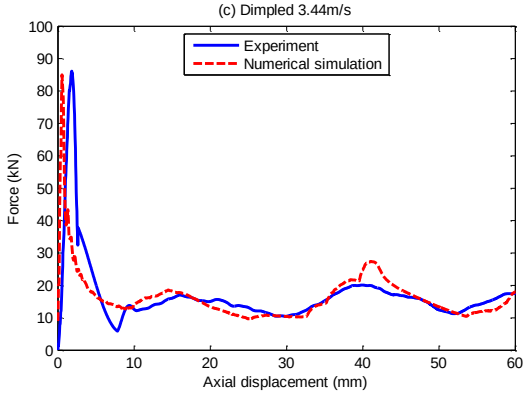
(c) Dimpled 3.44m/s
Experiment
Numerical simulation
Force (kN)
Axial displacement (mm)

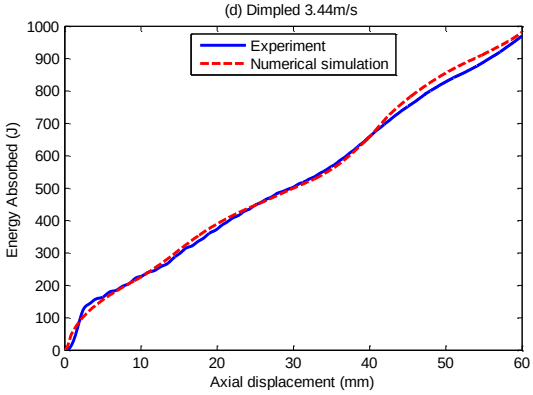
(d) Dimpled 3.44m/s
Experiment
Numerical simulation
Energy Absorbed (J)
Axial displacement (mm)

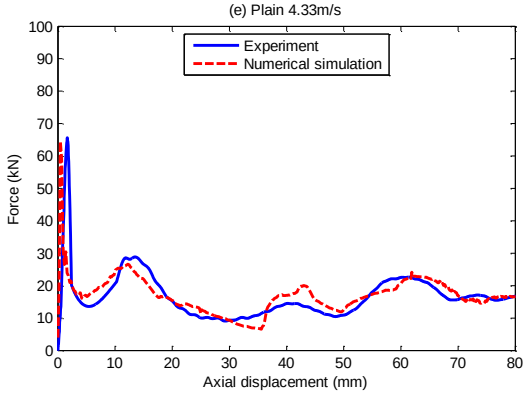
(e) Plain 4.33m/s
Experiment
Numerical simulation
Force (kN)
Axial displacement (mm)

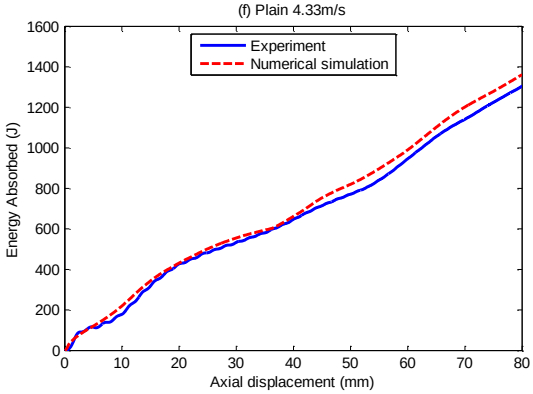
(f) Plain 4.33m/s
Experiment
Numerical simulation
Energy Absorbed (J)
Axial displacement (mm)

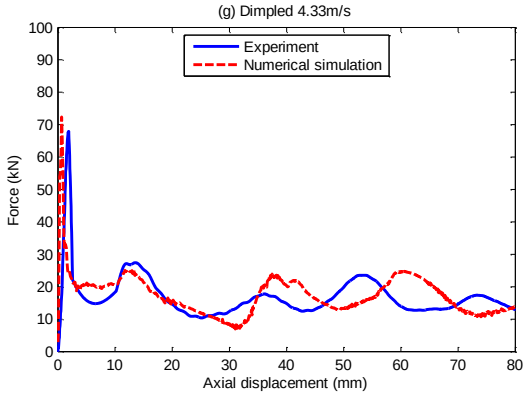
(g) Dimpled 4.33m/s
Experiment
Numerical simulation
Force (kN)
Axial displacement (mm)

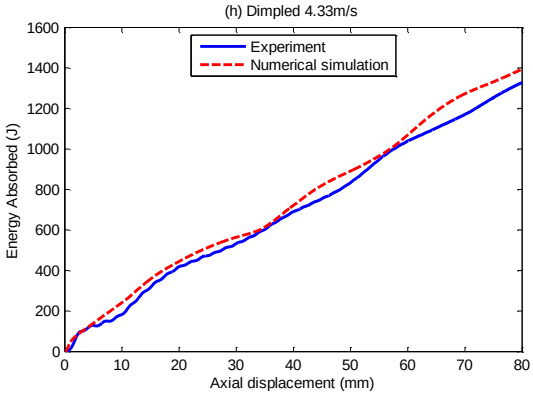
(h) Dimpled 4.33m/s
Experiment
Numerical simulation
Energy Absorbed (J)
Axial displacement (mm)

Fig. 14. Numerical and experimental force – displacement and energy absorbed – displacement curves for (a)(b) plain 3.44 m/s, (c)(d) dimpled 3.44 m/s, (e)(f) plain 4.33 m/s and (g)(h) dimpled 4.33 m/s

Table 2. Experimental results

Material	Impact velocity (m/s)	Mean crushing force P_m (kN)	SEA (kJ/kg)
Plain	3.44	14.342	11.437
Dimpled	3.44	15.835	12.628
Plain	4.33	14.234	11.351
Dimpled	4.33	15.519	12.376

For the impact velocities of 3.44 and 4.33 m/s, SEA of dimpled columns were 10.40% and 9.02% higher than those of plain columns, respectively. Moreover, as the impact velocity being increased from 3.44 to 4.33 m/s, SEA of plain and dimpled columns slightly dropped by 0.75% and 2.00%. This is due to the fact that initiators were only introduced in those tests with the impact velocity of 4.33 m/s.

3.2 Numerical results and validation

In this section, the FE method will be validated by comparing numerical with experimental results.

The numerical instantaneous force – displacement curves are shown in red in Fig. 15. It can be observed that the numerical and experimental results agreed very well. Most of the features in experiments were successfully captured in simulations, except for the initial peak. The difference before the initial peaks was due to the fact that Cowper-Symonds material model was used in simulations, where the materials were assumed to be perfectly plastic. The absence of elastic regions has resulted in an earlier appearance of initial peak force in simulations. Additionally, in those 3.44 m/s test

groups, the peak forces were slightly underestimated in simulations, because of the triggers used in simulations.

Numerical and experimental failure modes are shown in Fig. 15. All the numerical failure modes have been extended for 40mm to represent the un-deformed section clamped by the fixture in the experimental tests, as mentioned in section 2.1 and 2.2. The agreement was generally very good. However, simulations tend to slightly overestimate the folding wavelength. At the impact velocity of 3.44 m/s, the folding wavelengths were overestimated by 3.36% and 7.83% for plain and dimpled models, respectively. At the impact velocity of 4.33 m/s, the folding wavelengths were overestimated by 3.34% and 16.81% for plain and dimpled models, respectively.

This was also reflected on the number of formed folding layers. In Fig. 15(b), the second layer of folds has been fully formed in the experimental test, while the second layer of folds is still developing in the simulation. Similarly in Fig. 15(d), the formation of the third layer of folds has started in the experimental test, but not in the simulation. Even though the lengths of folds were slightly overestimated for dimpled columns, the SEA can still be accurately predicted. Table 3 shows numerical and experimental specific energy absorptions. It can be seen that the simulation errors are within 5%.

Table 3. Comparison of experimental and numerical SEA

Material	Impact velocity (m/s)	EXP SEA (kJ/kg)	FE SEA (kJ/kg)	Error
Plain	3.44	11.437	11.140	2.60%
Dimpled	3.44	12.628	12.113	4.08%
Plain	4.33	11.351	11.774	3.73%
Dimpled	4.33	12.376	12.818	3.57%

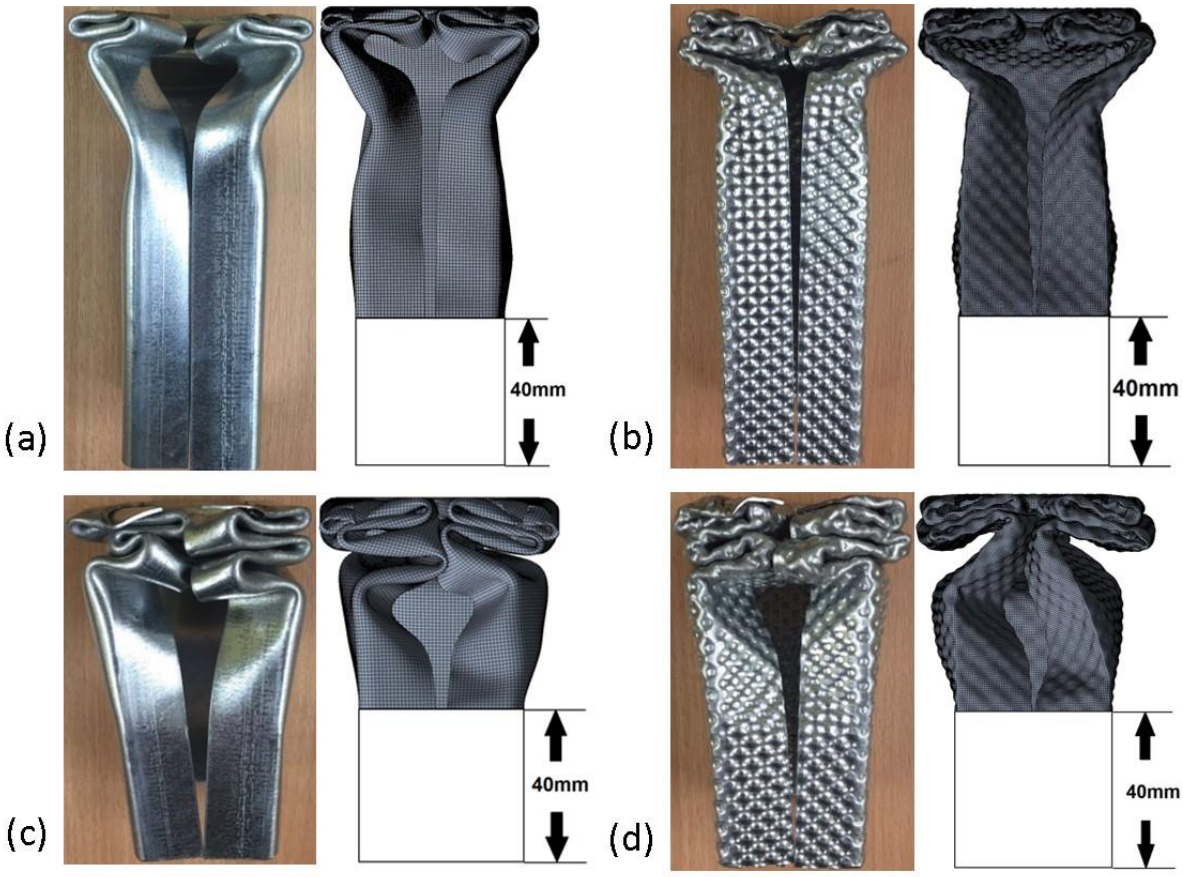

Fig. 15. Experimental and numerical failure modes of (a) plain 3.44 m/s, (b) dimpled 3.44 m/s, (c) plain 4.33 m/s and (d) dimpled 4.33 m/s

4. Optimization of the forming parameters

In the UltraSTEEL® forming process, forming depth is defined as the relative vertical movement between the upper and lower forming teeth, as indicated in Fig. 16. The forming depth and gauge thickness have a direct influence on the geometry of dimpled plates as well as material properties, which subsequently affects the energy absorption characteristics.

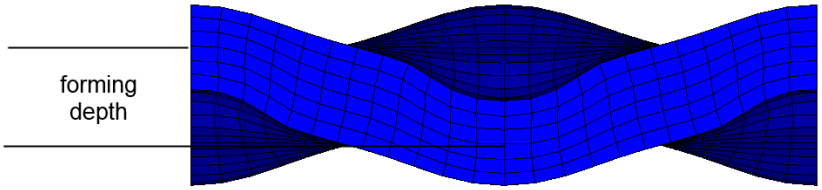

Fig. 16. Forming depth in the UltraSTEEL® forming process

4.1 Change in material properties due to forming parameters

During the forming process, work hardening is developed, which has caused an increase in the equivalent yield strength of the dimpled plate. However, this is not always valid as the forming depth increasing. Fig. 17. shows the variations of yield strengths against forming depths in dimpled plates for 0.8mm, 1.0mm and 1.2mm gauge thickness. It has been shown that the yield strengths tend to peak when the forming depth is approximately 1mm. The drop in yield strengths afterwards is caused by the stress concentrations due to the dimpled geometry. Fig. 18. shows the von-mises stress distribution in tensile tests. When a dimpled plate is being pulled, higher stress appears on the local areas, where yielding has initiated. In the meantime, the stress level on other areas remains low. In another word, the dimpled plate starts to

show globally yielding under tension while some areas are still in elastic region. This phenomenon outweighs the work hardening effect in the dimples when the forming depth is too high.

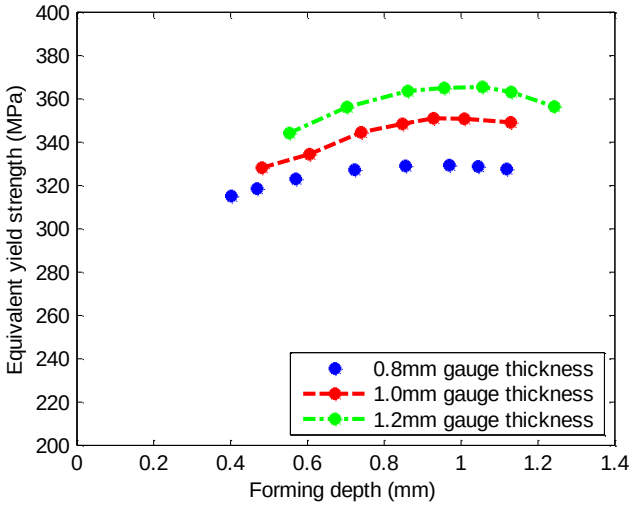

Fig. 17. Equivalent yield strengths vs forming depths

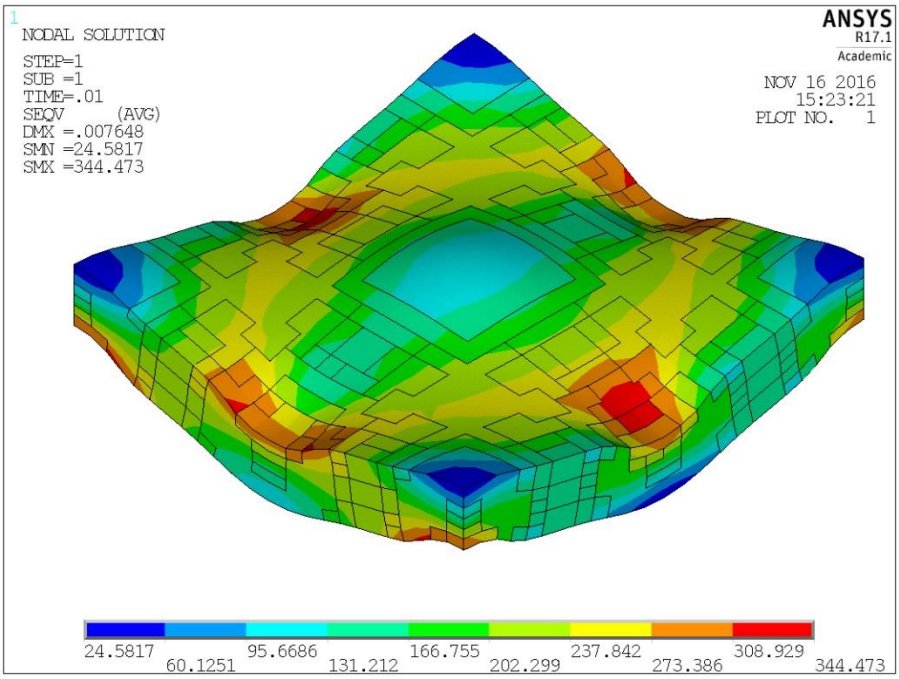

Fig. 18. Typical von-Mises stress distribution on a dimpled plate in tensile tests

4.2 Change in energy absorption due to forming parameters

Besides the effect on material properties, a greater forming depth means the plate is more stretched. Therefore the actual thickness of the dimpled plate becomes smaller and the geometry becomes more wavy. In order to understand its influence on the specific energy absorption (SEA), simulations were carried out on closed square dimpled columns, against plain columns with the same cross-section. As illustrated in Fig. 19, when the column subjected to axial impact loads, the folding mechanism and crushing force – axial displacement pattern are consistent to the square plain columns, which have already been fully described by Abramowicz et al. [1-3].

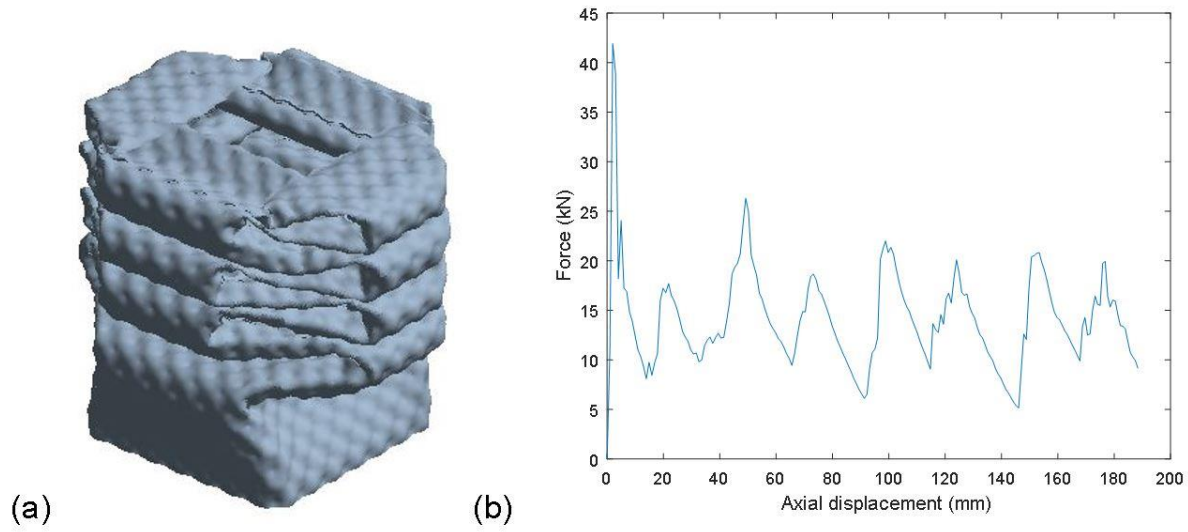

Fig. 19. Typical failure mode and crushing force vs axial displacement curve for closed square section dimpled columns

Fig. 20(a). shows the variations of SEA against forming depth of 0.7, 0.8, 0.9 and 1.0mm gauge dimpled columns. It was observed that SEA tends to peak. The drop in SEA after the peak point is due to the reduction in the actual thickness and the yield strength of the dimpled plates. In Fig. 20(b), SEA and forming depth were normalized using equation (5) and (6). Fig. 20(b). indicates that the optimal forming depth is

approximately 0.9 times of the gauge thickness, on the energy absorption front. For 0.7, 0.8, 0.9 and 1.0mm gauge dimpled columns, the maximum SEA are 10.4%, 13.7%, 14.9% and 16.3% higher than the corresponding plain ones.

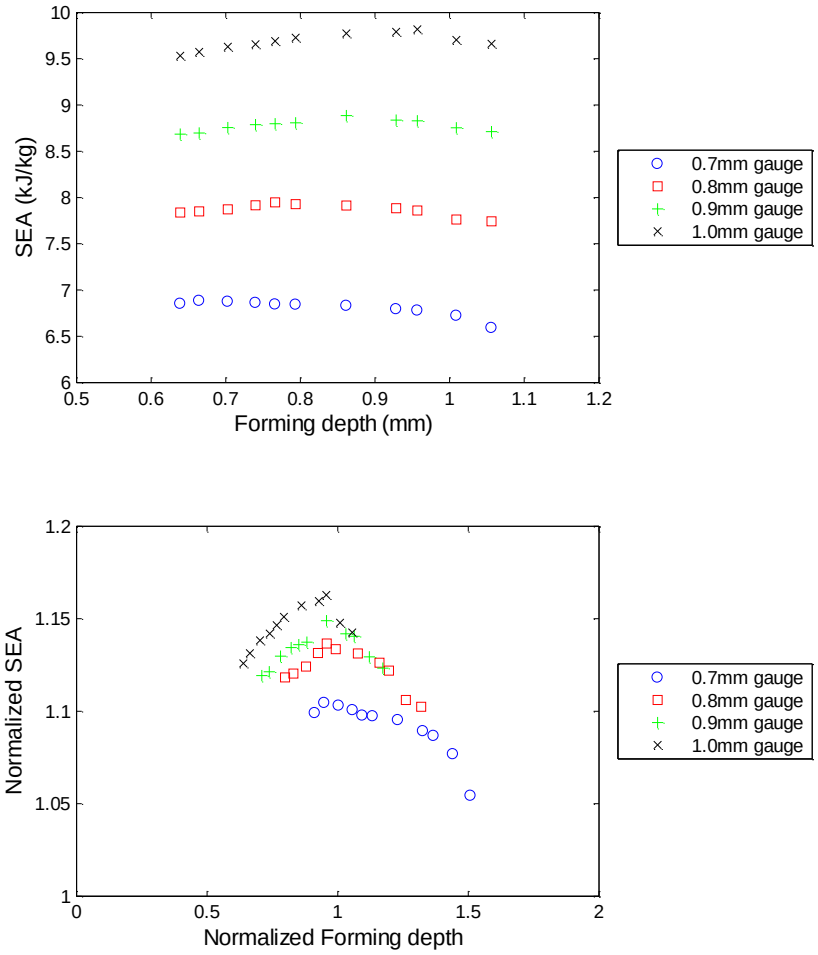

Fig. 20. (a) SEA vs Forming depth and (b) Normalized SEA vs Normalized Forming depth for 0.7, 0.8, 0.9 and 1.0mm gauge dimpled columns

$$Normalized\ SEA = \frac{SEA}{SEA\ of\ the\ original\ plian\ column} \tag{5}$$

$$Normalized\ forming\ depth = \frac{Forming\ depth}{Gauge\ thickness} \tag{6}$$

4. Conclusion

In this paper, experimental testing and finite element modelling were developed to predict the energy absorption characteristics of dimpled thin-walled structures when subjected to axial impact loads. This FE method was then validated by comparing numerical results with experimental results. Comparison analysis between plain and dimpled steel columns was also conducted. Dynamic crushing tests were conducted at two different impact velocities. These tests were replicated by running non-linear finite element explicit dynamics simulations.

In the simulations, the selection of element sizes for dimpled models mainly depends on the geometry. The effect of triggers was found to be more significant on dimpled models than on plain models, therefore triggers were necessary for the dimpled models. The open-section columns analysed in this study had a similar crushing mode with the conventional square closed section columns. Specific energy absorptions of dimpled columns are approximately 10% higher than plain columns with the same gauge thickness, under low-velocity axial impact loads. The numerical results agreed very well with experimental results in terms of instantaneous crushing force, failure mode and SEA values. Assumptions of uniform thickness and homogeneous material properties for modelling the dimpled models under axial impact loads were found to be appropriate.

Furthermore, the effect of the parameter of forming depth in the forming process has been studied. It was found that the forming depth has a non-linear influence on the yield strength and geometry, which subsequently affects the energy absorption performance. The optimization study indicated that dimpled plate’s yield strength peaks when forming depth is approximately 1mm, regardless of the gauge thickness.

The optimization study also indicated that the SEA of dimpled columns peaks when the forming depth is approximately 0.9 times of the gauge thickness. The increment on SEA is up to 16.3% for 1mm gauge dimpled columns.

References

[1] Wierzbicki T, Abramowicz W. On the Crushing Mechanics of Thin-Walled Structures 1983;50:727-734.

[2] Abramowicz W, Jones N. Dynamic axial crushing of square tubes. International Journal of Impact Engineering 1984;2(2):179-208.

[3] Abramowicz W, Jones N. Dynamic progressive buckling of circular and square tubes. International Journal of Impact Engineering 1986;4(4):243-270.

[4] Abramowicz W, Wierzbicki T. Axial crushing of multicorner sheet metal columns. Journal of Applied Mechanics ASME 1989;56(1):113-120.

[5] Tang Z, Liu S, Zhang Z. Energy absorption properties of non-convex multi-corner thin-walled columns. Thin-Walled Structures 2012;51:112-120.

[6] Abbasi M, Reddy S, Ghafari-Nazari A, Fard M. Multiobjective crashworthiness optimization of multi-cornered thin-walled sheet metal members. Thin-Walled Structures 2015;89:31-41.

[7] Reddy S, Abbasi M, Fard M. Multi-cornered thin-walled sheet metal members for enhanced crashworthiness and occupant protection. Thin-Walled Structures 2015;94:56-66.

[8] Jusuf A, Dirgantara T, Gunawan L, Putra IS. Crashworthiness analysis of multi-cell prismatic structures. International Journal of Impact Engineering 2015;78:34-50.

[9] Qiu N, Gao Y, Fang J, Feng Z, Sun G, Li Q. Crashworthiness analysis and design of multi-cell hexagonal columns under multiple loading cases. Finite Element in Analysis and Design 2015;104:89-101.

[10] Tran TN, Hou S, Han X, Tan W, Nguyen NT. Theoretical prediction and crashworthiness optimization of multi-cell triangular tubes. Thin-Walled Structures 2014;82:183-195.

[11] Tran TN, Hou S, Han X, Chau MQ. Crushing analysis and numerical optimization of angle element structures under axial impact loading. Composite Structures 2015;119:422-435.

[12] Zhang X, Zhang H. Some problems on the axial crushing of multi-cells. International Journal of Mechanical Sciences 2015;103:30-39.

[13] White M, Jones N, Abramowicz W. A theoretical analysis for the quasi-static axial crushing of top-hat and double-hat thin-walled sections. International Journal of Mechanical Sciences 1999;41:209-233.

[14] Ly HA, Nguyen HH, Thai-Quang T. Geometrical Optimization of Top-Hat Structures Subject to Axial Low Velocity Impact Load Using Numerical Simulations. International Journal of Mechanical Engineering and Applications 2015;3:40-48.

[15] Zhang X, Wen Z, Zhang H. Axial crushing and optimal design of square tubes with graded thickness. Thin-Walled Structures 2014;84:263-274.

[16] Huh H, Kang WJ. Crash-worthiness assessment of thin-walled structures with the high-strength steel sheet. International Journal of Vehicle Design 2002;30(1/2):1-21.

[17] Schneider F, Jones N. Impact of thin-walled high-strength steel structural sections. In: Proceedings of the Institution of Mechanical Engineering, Part D: Journal of Automobile Engineering; 2004;218(2):131-158.

[18] Tarigopula V, Langseth M, Hopperstad OS, Clausen AH. Axial crushing of thin-walled high-strength steel sections. International Journal of Impact Engineering 2006;32:847-882.

[19] Lam K, Behdinan K, Cleghorn W. A material and gauge thickness sensitivity analysis on the NVH and crashworthiness of automotive instrument panel support. Thin-Walled Structures 2003;41:1005-1018.

[20] Hanssen A, Langseth M, Hopperstad O. Static crushing of square aluminium extrusions with aluminium foam filler. International Journal of Mechanical Sciences 1999;41:967-993.

[21] Hanssen AG, Langseth M, Hopperstad OS. Static and dynamic crushing of square aluminium extrusions with aluminium foam filler. International Journal of Impact Engineering 2000;24:347-383.

[22] Zarei HR, Kroger M. Optimization of the foam-filled aluminium tubes for crush box applications. Thin-Walled Structures 2008;46:214-221.

[23] Hadley Industries plc, PO Box 92, Downing Street, Smethwick, West Midlands, B66 2PA, UK.

[24] Nguyen VB, Wang CJ, Mynors DJ, English MA, Castellucci MA. Dimpling process in cold roll metal forming by finite element modelling and experimental validation. Journal of Manufacturing Process 2014;16:363-372.

[25] Collins J, Castellucci MA, Pillinger I, Hartley P. The influence of tool design on the development of localised regions of plastic deformation in sheet metal formed products to improve structural performance. In: Proceedings of the tenth international conference on metal forming; 2004. p. 68.

[26] Nguyen VB, Wang CJ, Mynors DJ, English MA, Castellucci MA. Mechanical behaviour of cold-rolled formed dimpled steel. Steel Res Int 2011; Special Issue: 1072-1077

[27] Nguyen VB, Wang CJ, Mynors DJ, Castellucci MA, English MA. Finite Element simulation on mechanical and structural properties of cold-formed dimpled steel. Thin-Walled Structures 2013;64:13-22.

[28] Nguyen VB, Wang CJ, Mynors DJ, English MA, Castellucci MA. Compression tests of cold-formed plain and dimpled steel columns. Journal of Constructional Steel Research 2012;49:20-29.

[29] Nguyen VB, Mynors DJ, Wang CJ, Castellucci MA, English MA. Analysis and design of cold-formed dimpled steel columns using Finite Element techniques. Finite Elements in Analysis and Design 2016;108:22-31.

[30] BritishStandard, BS EN 10002-1:2001. Metallic materials – Tensile testing – Part 1: Method of test at ambient temperature; 2001.

[31] ANSYS® Academic Research, Release 16.0.